ELSEVIER

May 1994

Pattern Recognition Letters

Pattern Recognition Letters 15 (1994) 497–506

# Measurement of 3D-line shaped objects *

Marcel Worring [a,**], Pia Pfluger [a], Arnold W.M. Smeulders [a,b], Adriaan B. Houtsmuller [b]

[a] *Department of Mathematics and Computer Science, Univ. of Amsterdam, Amsterdam, Netherlands*
[b] *Department of Molecular Cell Biology, Univ. of Amsterdam, Amsterdam, Netherlands*

Received 15 July 1993; revised 1 October 1993

**Abstract**

We present a software tool for the analysis of 3D-line shaped objects in a 3D grey valued image. We discuss the extraction of the object from the image, the measurement of its shape features and its display.

*Key words*: 3D-curves; Shape measurement; Interactive visualization

## 1. Introduction

In 3D, one can distinguish objects bounded by a surface, such as cells, organs, and the skull, from objects which are tubular shaped. Examples of the latter are condensed chromosomes, blood vessels, and transport channels. The shape of the tubular objects is best described by the shape of the axis of the object which is a 3D-spatial curve.

Segmentation of such objects differs from the more usual 3D-volume segmentation as in, for example, Strasters and Gerbrands (1991). We use the "homing cursor", as described in Houtsmuller et al. (1993), to extract the axis of the line-shaped object from the image. This cursor automatically finds the axis between an interactively indicated start and end point, without reference to the surface bounding the object. The method assumes that the axis of the object is the local extremum of intensity. It traces the extremum until the indicated end point is reached. If in the course of the tracing, the algorithm reaches a point where there are two possible paths, it asks for interactive guidance from the user. The cursor yields an ordered set of 3D-points with sub-voxel accuracy as output.

The next step in the analysis is the shape measurement from the points on the axis found. The shape of this curve is captured by its bending and its twisting (related to the torsion of the curve). Estimation of these properties is a difficult task as it requires accurate estimation of higher order derivatives. Few methods for shape estimation of 3D-curves are found in the computer vision literature. In Mokhtarian (1988), only the theoretical aspects of the evolution of curves from progressive Gaussian smoothing of the coordinates are considered. As in the 2D-case (Lowe, 1988), Gaussian smoothing leads to a considerable shrinking of the curve, which cannot easily be corrected for as in the reference, because the shrinking in 3D depends on both the bending *and* the twisting of the curve. Practical aspects of 3D-curve shape are considered in Kehtarnavaz and deFigueiredo (1988a). They use one measure, the "structural variation" of the curve, which incorporates both the

* This work was supported by the Dutch Ministry of Economic Affairs through SPIN grants "3D Computer Vision" and "3D Image Analysis".

** Corresponding author. Email: worring@fwi.uva.nl


*SSDI* 0167-8655(93)E0096-7

bending and twisting properties of the curve. Points of high structural variation are used in the reference to define breakpoints on the curve. These breakpoints are the basis for the reconstruction of 3D-surfaces (Kehtarnavaz and deFigueiredo, 1988b). In Kehtarnavaz and deFigueiredo (1988a) the influence of noise is considered, but only its effects on the position and number of breakpoints.

The last step in the analysis is the display of the axis of the object. Displaying a 3D-curve to reveal its winding shape is a difficult visualization problem. Live rotation renders the best perceptual clue, but is of little help in hard copy publications. For that purpose we prefer a visualization offering a set of standardized orthogonal and simultaneous views. Such visualization captures the visual aspects of the object in a standard way.

A software tool for the analysis of line shaped space objects should contain all three steps mentioned above. In this paper we consider the shape estimation and visualization, we do not go into detail on the curve extraction (see Houtsmuller et al., 1993).

## 2. The shape of 3D-curves

We need some concepts from differential geometry, in particular the geometry of space curves. For more details, the reader is referred to text books (Struik, 1984). Let $\boldsymbol{x}(s)$ denote an arbitrary 3D-curve where $s$ is the arclength parameter along the curve. A frame field on $\boldsymbol{x}$ is a set of 3 vectors $\{\boldsymbol{e}_1, \boldsymbol{e}_2, \boldsymbol{e}_3\}$ defined for every point on $\boldsymbol{x}$ such that the vector $\boldsymbol{e}_i$ has unit length and is perpendicular to each of the vectors $\boldsymbol{e}_j$ if $i \neq j$. For description of the space curve shape, the Frenet frame, see Fig. 1, is the natural choice. The first vector of the frame is the tangent $\boldsymbol{t}(s)$ of the curve. The second vector $\boldsymbol{n}(s)$ is the unit normal of the curve. The third vector is the binormal $\boldsymbol{b}(s)$ defined as the vector product of the tangent and the normal.

The shape of the curve is completely characterized by the changing of the Frenet frame $\{\boldsymbol{t}, \boldsymbol{n}, \boldsymbol{b}\}$ when we move along the curve. The changes are given by:

$$\boldsymbol{t}' = \kappa \boldsymbol{n} ,$$

$$\boldsymbol{n}' = -\kappa \boldsymbol{t} + \tau \boldsymbol{b} ,$$

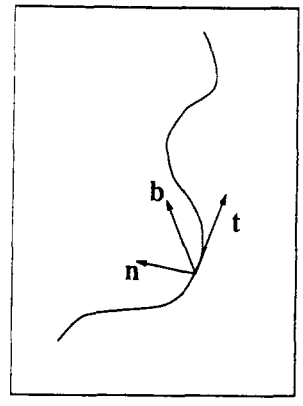


Fig. 1. The Frenet frame on a curve is a local frame of reference, defined by the tangent $\boldsymbol{t}$, the normal $\boldsymbol{n}$ and the binormal $\boldsymbol{b}$.

$$\boldsymbol{b}' = -\tau \boldsymbol{n} . \tag{1}$$

The functions $\kappa(s)$ and $\tau(s)$ are the curvature and the torsion of the curve, respectively. The curvature measures the deviation of the curve from being straight, whereas the torsion measures the deviation from being a planar curve. The fundamental theorem in the differential geometry of curves states that if curvature and torsion are known as function of arclength then we can reconstruct the curve up to a rigid transformation. Hence, the curvature and torsion capture all of the shape information of the curve. For the arclength parameterized curve they are given by:

$$\kappa = \|\boldsymbol{x}''\|, \qquad \tau = \frac{(\boldsymbol{x}'\boldsymbol{x}''\boldsymbol{x}''')}{\kappa^2} \tag{2}$$

where $(\boldsymbol{x}'\boldsymbol{x}''\boldsymbol{x}''')$ is the triple scalar product, whose absolute value gives the volume of the parallelepiped spanned by the three derivative vectors.

Note that curvature is always positive, in contrast to the curvature of curves in 2D where it is given a sign distinguishing convex from concave regions. For 3D-curves the notions concave and convex do not apply as one cannot discriminate between the inside and outside of the object as in the 2D-case. We describe the bending properties of the curve by the local bending energy $BE$.

At positions where the curvature vanishes, torsion is not defined. Therefore, we prefer to use the derivative volume as a measure $TW$ for the twisting of the curve. This measure has the same sign as the torsion, but at (almost) straight parts of the curve it is forced to zero. So we have:

$$BE=\kappa^2, \qquad TW=\kappa^2\tau\,. \tag{3}$$

The local behavior of a curve is revealed by considering the movement of the Frenet frame along the curve, expressed in its own coordinate frame. In the Frenet frame with coordinates $(x_f, y_f, z_f)$, the following relationships can be derived from Eq. (1) by taking the first-, second- and third-order derivative with respect to $\boldsymbol{t}$, $\boldsymbol{n}$, and $\boldsymbol{b}$, respectively, see Struik (1984):

$$\begin{aligned} &x_f'=1, && y_f'=0, && z_f'=0\,,\\ &x_f''=0, && y_f''=\kappa, && z_f''=0\,,\\ &x_f'''=-\kappa^2, && y_f'''=\kappa', && z_f'''=\kappa\tau\,. \end{aligned} \tag{4}$$

The formulae indicate that in first order, the movement of the curve is along $x_f$, that is the tangent, only. In second order, the movement is in the direction of the normal only. These two movements follow from the definition of the Frenet frame, really. In third order the torsion comes in. In lowest-order approximation for the small changes of $s$, we arrive at the following well known relations between the Frenet coordinates for any smooth curve:

$$y_f=\frac{\kappa}{2}x_f^2, \qquad z_f=\frac{\kappa\tau}{6}x_f^3, \qquad z_f^2=\frac{2\tau^2}{9\kappa}y_f^3\,. \tag{5}$$

Consequently, the local projection of any smooth space curve on the tangent–normal plane is a parabola with width determined by curvature. In contrast, the projection on the tangent–binormal plane is a curve of degree 3. Depending on the sign of $\tau$ the curve goes through the local origin with negative or positive slope. The projection on the normal–binormal plane is a curve with a cusp in the local origin (see Fig. 2a).

The approximations are valid only if both $\kappa\neq 0$ and $\tau\neq 0$. If $\kappa=0$ the curve degenerates locally into a straight line and the Frenet frame is not defined. However, if the torsion vanishes and the change of torsion does not, we need to consider higher-order terms in the local approximation of the curve. In Worring (1993) it is shown that the projections become:

$$y_f=\frac{\kappa}{2}x_f^2, \qquad z_f=\frac{\kappa\tau'}{24}x_f^4, \qquad z_f=\frac{\tau'}{6\kappa}y_f^2\,. \tag{6}$$

It follows that the characteristics of the projection in the tangent–normal plane do not change as compared to the case of non-vanishing torsion. However, in the tangent–binormal plane the curve does not change sign in the origin any longer, but is locally either positive or negative depending on the sign of the change of torsion. In the normal–binormal plane

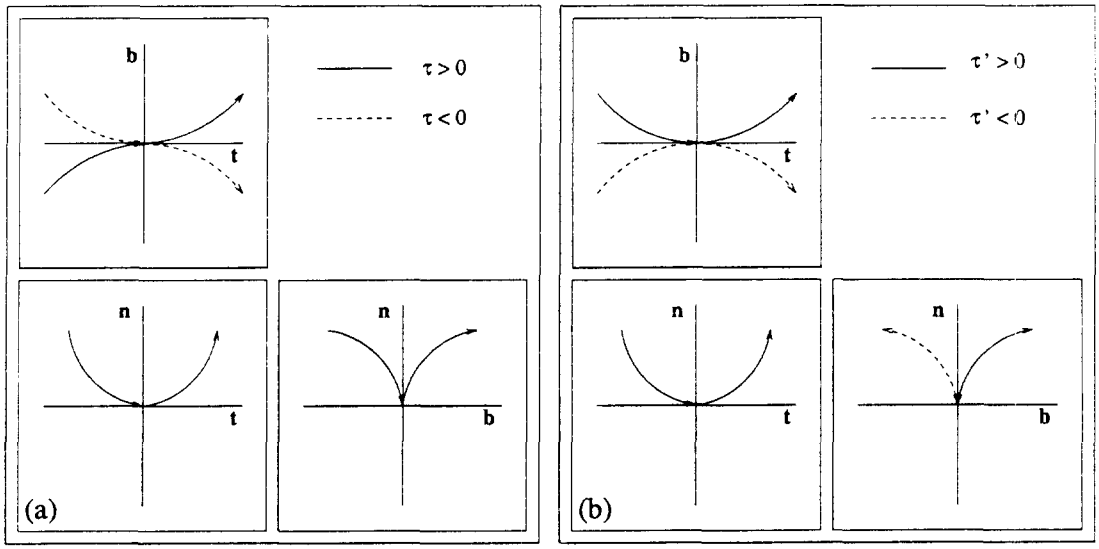


Fig. 2. Schematic drawing of the projections of an arbitrary curve on the planes defined by the local Frenet frame for a curve which locally has $\tau\neq 0$ (a) and a curve with $\tau=0$ (b).

the curve again has a cusp, but the curve leaves the cusp the same way it entered (see Fig. 2b). These aspects of the curve will be used in the display of the 3D-curve.

## 3. Curve approximation and shape measurement

The result of the line finding algorithm is given as a set of 3D-digital points $\{\boldsymbol{v}_i\}_{i=1,\ldots,n}$, representing some continuous curve $\boldsymbol{x}$. To be precise:

$$\{\boldsymbol{v}_i\}_{i=1,\ldots,n} = \boldsymbol{x}(i) + \tilde{\boldsymbol{\epsilon}}(i) \,. \tag{7}$$

The vector $\tilde{\boldsymbol{\epsilon}}(i)$ gives the deviation of the observed position of a point from its true position on the curve. The characteristics of $\tilde{\boldsymbol{\epsilon}}$ depend on the method of deriving the curve from the image. For the "homing cursor", which measures positions with sub-voxel accuracy, systematic influences in the noise due to digitization effects are neglectible. So, adoption of a stochastic noise model is appropriate.

Given the noise-corrupted points $\boldsymbol{v}_i$, our goal is to find estimates $\{\hat{\boldsymbol{t}}, \hat{\boldsymbol{n}}, \hat{\boldsymbol{b}}\}$ of the local Frenet frame and shape estimates $\widehat{BE}$ and $\widehat{TW}$. To that end one needs accurate estimates of the derivatives of the curve up to third order.

We pose the shape estimation problem as a curve estimation problem: find a curve $\hat{\boldsymbol{x}}$ approximating the "true" curve $\boldsymbol{x}$ as faithfully as possible. From there, shape is calculated from the parameters of the fitted curve.

In order to calculate the approximation one has to define a mapping $t(\cdot)$ associating with every $i$-value a parameter value $t_i$ (commonly called a knot). It defines the correspondence between a data point and one point on the estimated curve. If the points $\boldsymbol{x}(t_i)$ arise from some physical phenomenon where parameter $t$ measures time for example, the choice of $t_i$ is obvious. This is less so in the case of a space curve derived from an image. Ideally, $t$ equals the arclength parameter of the underlying true curve. This true curve is not known, however. We use the arclength of the polygon through the points $\boldsymbol{v}$:

$$t(i) = \sum_{j=2}^{i} \|\boldsymbol{v}_j - \boldsymbol{v}_{j-1}\| \,. \tag{8}$$

In the absence of noise the estimated curve should interpolate the data, i.e. $\hat{\boldsymbol{x}}(t(i)) = \boldsymbol{v}_i$, in the smoothest way. If noise is present, however, such an interpolating curve could yield unreliable shape estimates. It is then natural to introduce two terms that must be minimized simultaneously, one for the distance between corresponding points and one which favors smooth estimates with a parameter $\lambda$ regulating the relative weight among the two. For 1D-function estimation it is common to bound a high-order derivative of the curve to control smoothness (Shahraray and Anderson, 1989; Woltring, 1986). Extending the methods in the references, we can pose the curve estimation problem as follows:

$$\hat{\boldsymbol{x}}_\lambda = \arg\min_{\hat{\boldsymbol{x}}} \left\{ \frac{1}{n} \sum_{i=1}^{n} \|\hat{\boldsymbol{x}}(t(i)) - \boldsymbol{x}_i\|^2 + \frac{\lambda}{(\delta t)^{2m-1}} \int_{t(1)}^{t(n)} \|\hat{\boldsymbol{x}}^{(m)}(u)\|^2 \, \mathrm{d}u \right\} \tag{9}$$

where $\delta t = t(n) - t(1)$. This term is introduced to make the estimated shape for fixed $\lambda$ independent of linear rescaling of the parameter $t$ (for example, to normalize to the interval $[0,1]$). The approximating curve $\hat{\boldsymbol{x}}$ is restricted to the class of functions having $m-1$ continuous derivatives and square integrable $m$th derivative.

The solution of Eq. (9) can be computed independently for each of the coordinates once the mapping $t(\cdot)$ is computed from Eq. (8). Each coordinate yields a smoothing spline of order $2m$, with simple knots at every $t(i)$. Between knots, such a spline is a polynomial of degree $2m-1$ at the most. At the knots the polynomials are joined such that the first $2m-2$ derivatives of the curve are continuous. At the end points of the interval the derivatives of order $\geqslant m$ vanish.

There are two parameters to be set at this point: the parameter $m$ governing the order of the curve ($=2m$), and the smoothing parameter $\lambda$.

The choice of $m$ is a compromise between the flexibility of the spline curve and the control over its smoothness. Using high-order splines allows faithful tracing of all possible bends and twists of the curve. Lower-order splines, however, are less affected by noise in the data and hence one has better control over their smoothness. Cubic splines ($m=2$) are not flex-

ible enough for space curves as torsion vanishes at every knot $t_i$. With $m=3$ the curve has smoothly varying curvature and torsion at the knots, but at the end points the torsion is forced to zero. We therefore use $m=4$, i.e. an 8th order spline, which is the lowest-order spline having smoothly varying shape with no predetermined curvature or torsion at end points.

In the current program the value of $\lambda$ is set interactively. Automated methods based on cross-validation (Shahraray and Anderson, 1989) do not apply in the current context (see Worring, 1993). In the interactive setting it is important for the user to have an immediate visual feedback on the consequences of using this particular value of $\lambda$. To that end, for a chosen $\lambda$, the system shows both the estimated shape as well as the smoothed curve. It is our experience that one quickly chooses a reasonable value of the parameter.

The result of approximation, captured in the points $\boldsymbol{c}_{i,\lambda}$ and the knots $t_i$, for properly chosen $\lambda$, is an analytical representation of the curve best approximating the data. Hence, the Frenet frame and shape features can be calculated analytically.

## 4. Experiments

### 4.1. Experimental setup

We performed Monte Carlo experiments to establish the quality of the curve approximation as presented in the previous section for the purpose of shape measurement. The natural test curve for experiments is the helix which has constant curvature and torsion. In its standard form (winding along the $z$-axis) the helix is given by:

$$\boldsymbol{x}(u) = (a\cos u,\ a\sin u,\ bu)\ , \tag{10}$$

where $a$ is the radius of the cylinder the helix clings to, and $b$ is the pitch of the helix. The curvature and torsion are given by:

$$\kappa = \frac{a}{a^2+b^2}\ , \qquad \tau = \frac{b}{a^2+b^2}\ . \tag{11}$$

The length $l$ of the path traversed by the helix for $u\in[u_0, u_1]$ equals

$$l = (u_1-u_0)\sqrt{a^2+b^2}\ . \tag{12}$$

The equation is used to obtain $N$ approximate unit length samples on the curve (i.e. $h\approx h_{\text{grid}}$) for parameter range $u=u_1-u_0$. Using $b=\nu a$ we find the relations:

$$a = \frac{N}{u\sqrt{\nu^2+1}}\ , \qquad b=\nu a\ . \tag{13}$$

In the experiment three helices of different radius and pitch are employed, defined by $\nu=\frac{1}{3}$, 1 and 3, respectively. With $u=2\pi$ and $N=50$ we find the respective $(a, b)$ pairs: (7.55, 2.52), (5.63, 5.63), and (2.52, 7.55). The axes of the helices have one arbitrarily chosen orientation (see Fig. 3).

We perform Monte Carlo experiments on the basis of Eq. (7), with the following expression for the noise:

$$\tilde{\boldsymbol{\epsilon}}_\gamma(i) = \tilde{r}_i\cos\tilde{\theta}_i\,\boldsymbol{n}(i) + \tilde{r}_i\sin\tilde{\theta}_i\,\boldsymbol{b}(i)\ , \tag{14}$$

where $\tilde{r}_i$ is zero-mean normally distributed independent noise with standard deviation $\gamma$. The angle $\tilde{\theta}_i$ has uniform distribution for each $i$. The parameter $\gamma$ var-

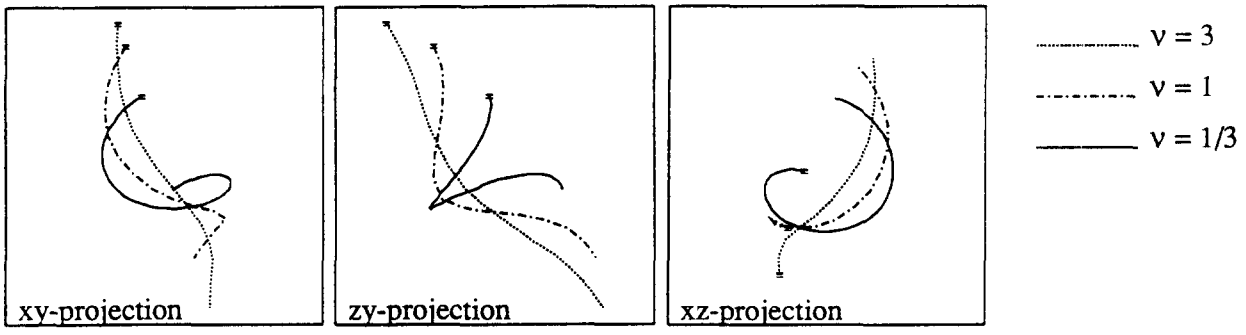


Fig. 3. The three helices used in the experiment, corresponding to different ratios $\nu$.

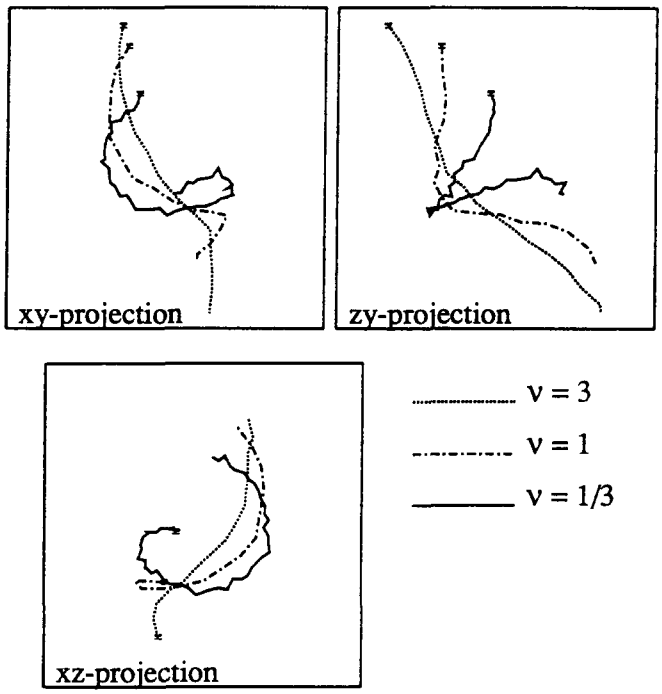


Fig. 4. One realization of the curves with noise ($\gamma=0.5$).

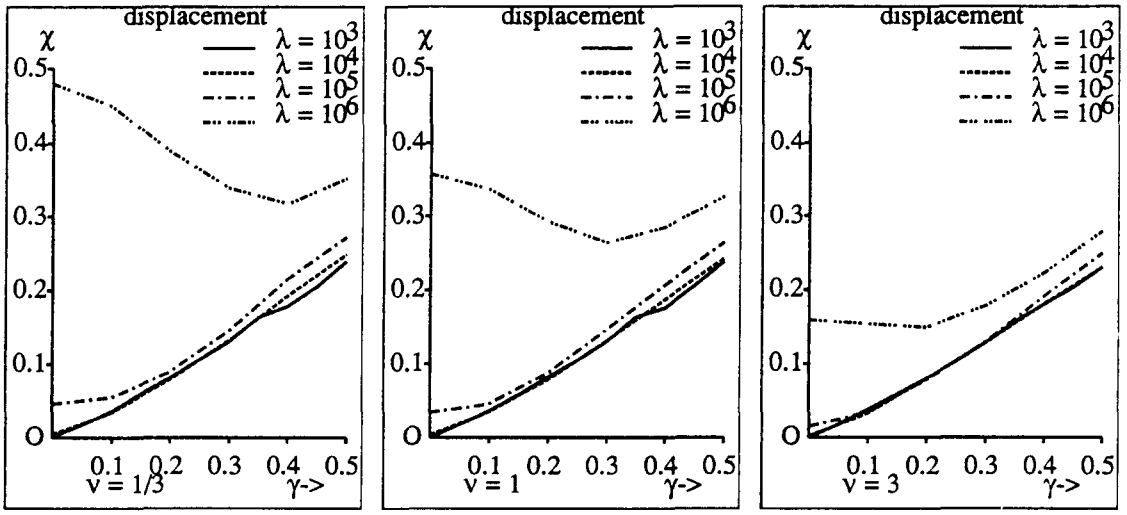


Fig. 5. The average displacement of the estimated points on the smoothed curve with respect to the corresponding true data points, i.e., prior to the addition of noise. Results are shown for the three helices $\nu=\frac{1}{3}$, 1 and 3.

ies between $0.0h$ and $0.5h$. In Fig. 4 an example noisy curve is shown. $K=100$ realizations of the noise are used for each experiment. For each realization the curve is reparameterized by the length of the line through the noisy datapoints.

The measure $\chi$ is the square root of the average displacement of all $K \cdot N=5000$ datapoints with respect to their position in the smoothed curve. To avoid endpoint effects the helices are extended to both sides with one full period

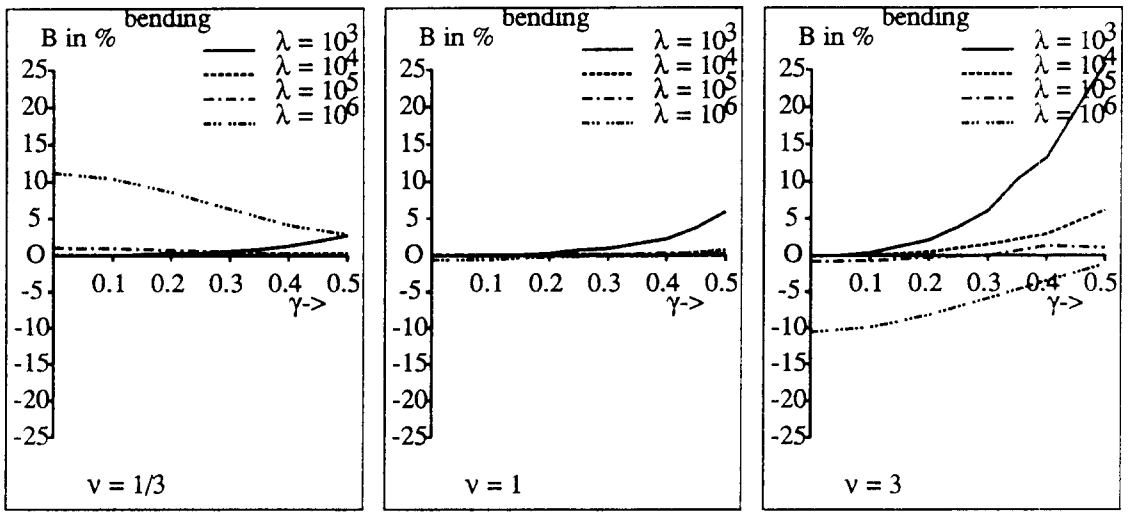


Fig. 6. The bias $B$ in the estimation of the bending energy $BE$ of the curve for the three helices, relative to the corresponding true value of $BE$.

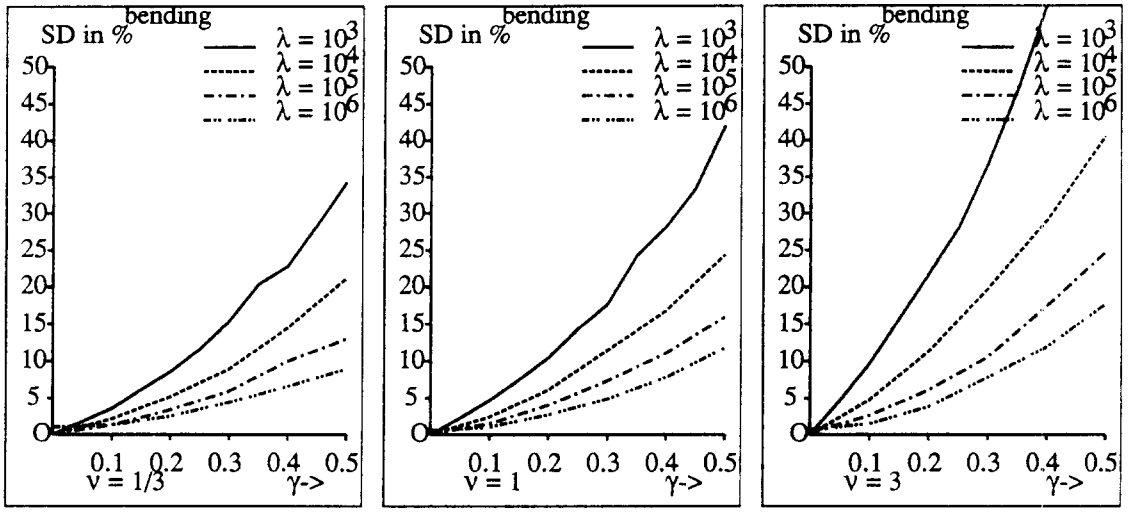


Fig. 7. The deviation $SD$ in the estimation of the bending energy of the helices, relative to the true value.

$$\chi^2_\lambda(\gamma)=\frac{1}{K\cdot N}\sum_{i=1}^{K}\sum_{j=1}^{N}\|\boldsymbol{v}_{\text{true}}(i)-\hat{\boldsymbol{x}}_{\lambda,\gamma}(t_i)\|^2 . \qquad (15)$$

In Fig. 5 the results are shown for different values of $\lambda$.

For every datapoint we calculate the shape descriptors (denoted by $BE$ and $TW$, see Eq. (3)) from the fitted curve. As a measure of performance of the shape measures the bias $B$ and the deviation $SD$ in the shape estimate are defined by:

$$B_\lambda(\gamma)=\frac{1}{K\cdot N}\sum_{i=1}^{K}\sum_{j=1}^{N}\{\widehat{BE}_{\lambda,\gamma}(t_i)-BE_{\text{true}}\} , \qquad (16)$$

$$SD^2_\lambda(\gamma)=\frac{1}{K\cdot N}\sum_{i=1}^{K}\sum_{j=1}^{N}\{\widehat{BE}_{\lambda,\gamma}(t_i)-\overline{BE}_{\lambda,\gamma}\}^2 , \qquad (17)$$

where $\overline{BE}$ is the average estimate obtained for the given $\lambda$ and $\gamma$. Formulae for $TW$ are likewise. Results are shown in Figs. 6–9.

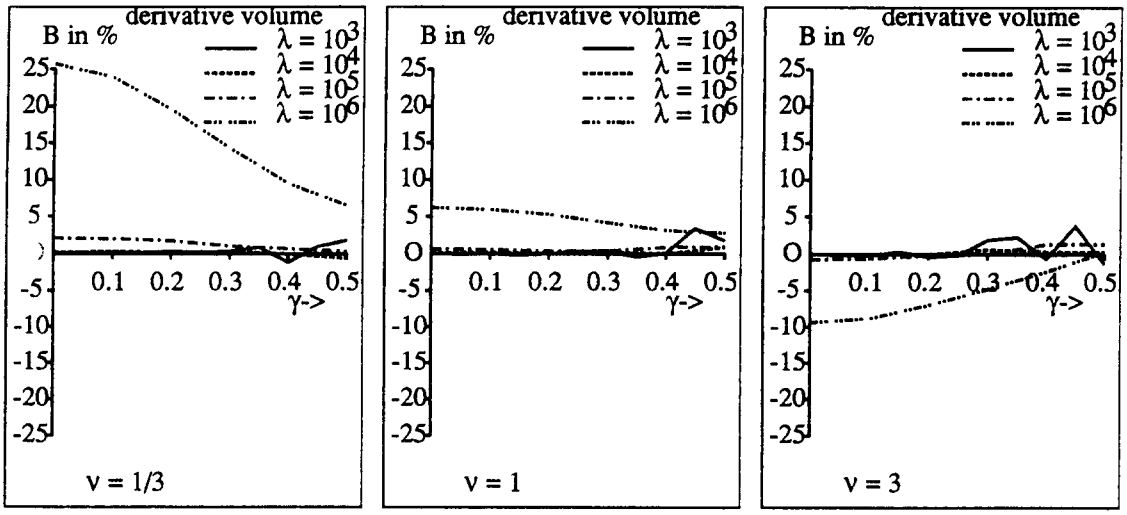


Fig. 8. The bias in measuring the derivative volume *TW*.

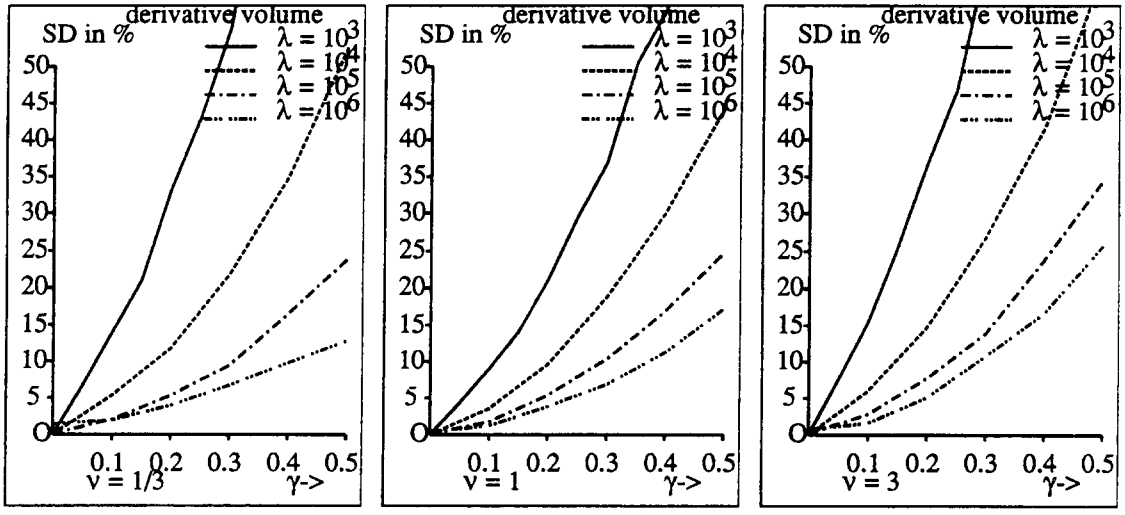


Fig. 9. Deviation in measuring the derivative volume, *TW*.

### 4.2. Discussion of the experiments

The results on the displacement of the curve in Fig. 5 show that displacement of the curve is small for all values of $\lambda < 10^5$. On the other hand, Figs. 6 and 7 show that the smallest measurement errors are found for the largest value of $\lambda$. Taking a strong damping factor of $\lambda = 10^6$ leads to the smallest deviations in the shape measures, for a noise-free curve at the prize of severe displacement of the points from their true position. It is the shrinking effect known from the Gaussian smoothing in 2D. The displacement is reflected in the bias of the shape measures. A choice of $\lambda = 10^3$ hardly leads to any displacement, but now the standard deviation of the shape measures is high.

With appropriate $\lambda$ (for our experimental setup $\lambda = 10^4$ or $\lambda = 10^5$ for small amounts of noise or $\lambda = 10^6$ for $\gamma > 0.4$) the displacement is small and shape measures are almost unbiased.

The standard deviation shows similar characteristics for all $\lambda$ considered. As expected the deviation is higher in the estimation of the derivative volume as it requires the use of third-order derivatives.

We conclude that for the purpose of quantitative

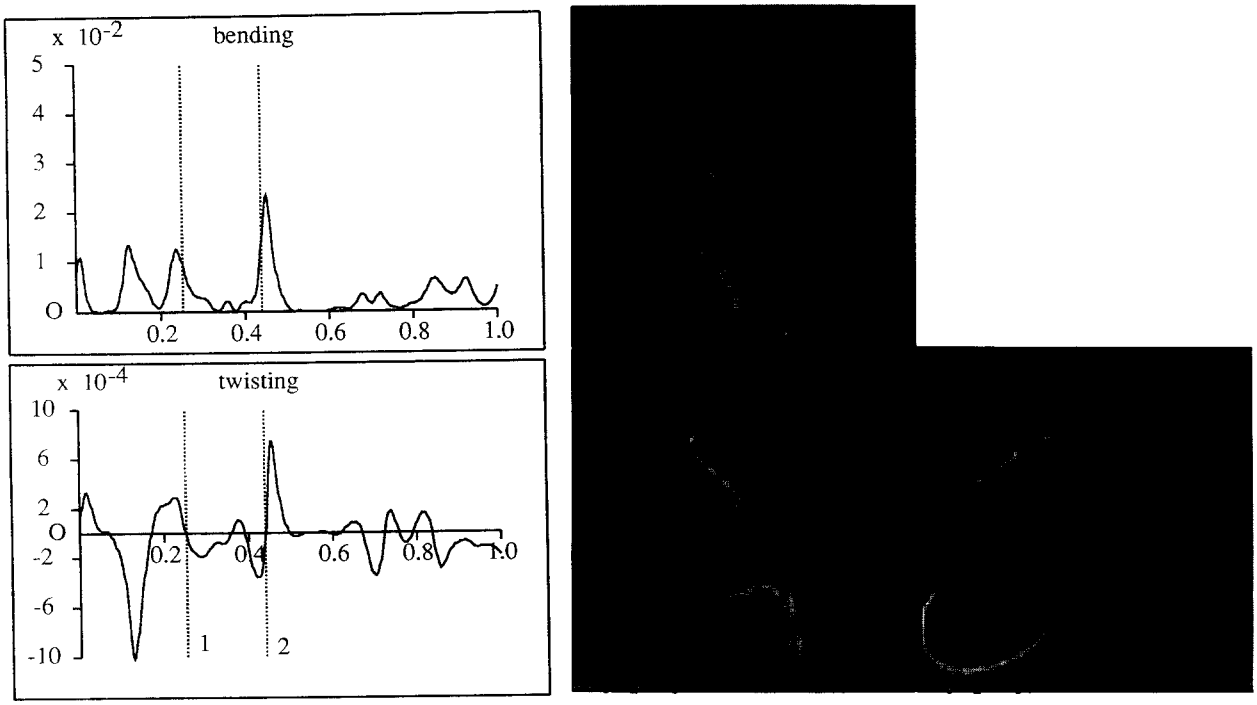


Fig. 10. Typical output of the system showing a 3D-image of an individual chromosome, selected from a 3D confocal microscopy scan. The viewport selected for display corresponds to the Frenet trihedron of the zero-crossing of the twisting labelled 1. In this standardized way of displaying 3D-curves, bending properties are seen in the tangent–normal plane, whereas twisting properties are visualized in the tangent–binormal plane. The actual rendering technique of the tube representation of the line is a volume renderer known as Simulated Fluorescence Process (van der Voort et al., 1993).

shape measurement the curve approximation yields reliable results for reasonable amounts of noise. It should be born in mind that the conclusion is limited, however, to curves of constant curvature and torsion. For a more general conclusion one should also include figures with zero-crossings in the torsion function as such zero-crossings might yield important shape information for 3D-curves.

## 5. Conclusion

The analysis of 3D-line shaped objects in an image consists of three steps. Extraction of the axis of the object, estimation of shape features, and display of the curve.

We have traced the axis with sub-voxel accuracy as in Houtsmuller et al. (1993) which is important for reliable shape estimation.

For the shape estimation we have presented a method based on smoothing splines which make a compromise between the displacement of the data points and the smoothness of the curve. The results of estimation yields an analytical curve, hence shape features and the Frenet frame can be calculated from the spline parameters. The experimental results show that with appropriate sub-voxel tracing, reliable estimates of shape can be obtained.

For 3D-curves, the method of display should be considered as a standard part of the analysis, as the 3D- to 2D-projection may distort the impression of the observer considerably. Therefore, we suggest to do so in a standard way, using three orthogonal projections. The Frenet frame provides such a standard for display, where the local bending of the curve can be seen in the tangent–normal plane and the twisting of the curve is displayed in the tangent–binormal plane. Note that such a method of display requires the analysis of the shape of the curve as the Frenet plane depends on the local shape of the curve. The

system is illustrated in Fig. 10. The figure gives the output for an image of a chromosome, where the viewpoint corresponds to one of the zero-crossings in the twisting of the curve (compare Fig. 2).

## 6. Acknowledgement

The authors wish to thank the anonymous referee for the effort to clarify the presentation of the paper.

## 7. References

Houtsmuller, A.B., A.W.M. Smeulders, H.T.M. van der Voort, J.L. Oud and N. Nanninga (1993). The homing cursor: a tool for three-dimensional chromosome analysis. *Cytometry* 14, 501–509.

Kehtarnavaz, N and R.J.P. deFigueiredo (1988a). A 3-D contour segmentation scheme based on curvature and torsion. *IEEE Trans. Pattern Anal. Machine Intell.* 10 (5), 707–713.

Kehtarnavaz, N and R.J.P. deFigueiredo (1988b). A framework for surface reconstruction from 3-D contours. *Computer Vision, Graphics, and Image Processing* 42, 32–47.

Lowe, D.G. (1988). Organization of smooth image curves at multiple scales. *Proc. Second Internat. Conf. on Computer Vision*, Tampa, 558–567.

Mokhtarian, F. (1988). Evolution properties of space curves. *Proc. Second Internat. Conf. on Computer Vision*, Tampa, 100–105.

Morse, B.S., S.M. Pizer and A. Liu (1993). Multiscale medial analysis of medical images. In: H. Barrett and A. Gmitro, Eds., *Information Processing in Medical Imaging.*

Shahraray, B. and D.J. Anderson (1989). Optimal estimation of contour properties by cross-validated regularization. *IEEE Trans. Pattern Anal. Machine Intell.* 11 (6), 600–610.

Strasters, K.C. and J.J. Gerbrands (1991). Three-dimensional image segmentation using a split, merge and group approach. *Pattern Recognition Lett.* 12, 307–325.

Struik, D.J. (1984). *Lectures on Classical Differential Geometry.* Dover, New York.

van der Voort, H.T.M, J.M. Messerli, H.J. Noordmans and A.W.M. Smeulders (1993). Volume visualization for interactive microscopic image analysis. *Bioimaging* 1, 20–29.

Woltring, H.J. (1986). A Fortran package for generalized cross-validatory spline smoothing and differentiation. *Adv. Eng. Software.* 8 (2), 104–113.

Worring, M. (1993). Shape Analysis of Digital Curves. PhD thesis, University of Amsterdam.